LYMPHOID NEOPLASIA

Loss of PRDM11 promotes MYC-driven lymphomagenesis

Cathrine Kolster Fog,[1] Fazila Asmar,[2] Christophe Côme,[1] Klaus Thorleif Jensen,[1] Jens Vilstrup Johansen,[1] Tony Bou Kheir,[1] Linda Jacobsen,[1] Carsten Friis,[1] Alison Louw,[1] Louise Rosgaard,[1] Nina Friesgaard Øbro,[3] Hanne Vibeke Marquart,[3] Kristian Anthonsen,[4] Arie Koen Braat,[5] Maarten van Lohuizen,[5] Elisabeth Ralfkiaer,[6] Kirsten Grønbæk,[1,2] and Anders Henrik Lund[1]

[1]Biotech Research and Innovation Centre and Centre for Epigenetics, University of Copenhagen, Copenhagen, Denmark; [2]Department of Hematology, [3]Department of Clinical Immunology, and [4]Department of Otorhinolaryngology, Head and Neck Surgery and Audiology, Copenhagen University Hospital, Rigshospitalet, Copenhagen, Denmark; [5]Division of Molecular Genetics, Netherlands Cancer Institute, Amsterdam, The Netherlands; and [6]Department of Pathology, Rigshospitalet, Copenhagen, Denmark

Key Points

- Loss of *Prdm11* accelerates MYC-driven lymphomagenesis.
- PRDM11 regulates transcription of target genes, including *FOS* and *JUN*.

The PR-domain (PRDM) family of genes encodes transcriptional regulators, several of which are deregulated in cancer. By using a functional screening approach, we sought to identify novel tumor suppressors among the PRDMs. Here we demonstrate oncogenic collaboration between depletion of the previously uncharacterized PR-domain family member *Prdm11* and overexpression of MYC. Overexpression of PRDM11 inhibits proliferation and induces apoptosis. *Prdm11* knockout mice are viable, and loss of *Prdm11* accelerates MYC-driven lymphomagenesis in the *Eμ-Myc* mouse model. Moreover, we show that patients with PRDM11-deficient diffuse large B-cell lymphomas (DLBCLs) have poorer overall survival and belong to the nongerminal center B-cell–like subtype. Mechanistically, genome-wide mapping of PRDM11 binding sites coupled with transcriptome sequencing in human DLBCL cells evidenced that PRDM11 associates with transcriptional start sites of target genes and regulates important oncogenes such as *FOS* and *JUN*. Hence, we characterize PRDM11 as a putative novel tumor suppressor that controls the expression of key oncogenes, and we add new mechanistic insight into B-cell lymphomagenesis. (*Blood*. 2015;125(8):1272-1281)

Introduction

PR-domain (PRDM) family members are transcriptional regulators with important roles in cell-fate specification.[1,2] The PRDM family consists of 17 members[3,4] and is characterized by the presence of a PR domain related to the SET domain found in histone lysine methyl transferases (HMTases).[5] Several family members have been shown to be intrinsic HMTases.[6-9] Furthermore, a number of PRDMs exhibit tumor suppression functions: for example, PRDM1 is a tumor suppressor of diffuse large B-cell lymphomas (DLBCLs),[10,11] whereas PRDM5 is a tumor suppressor of gastrointestinal carcinogenesis.[12,13]

One of the most well-characterized proto-oncogenes is the transcription factor MYC, which is deregulated in various cancers, including non-Hodgkin lymphomas.[14] *MYC* rearrangement is a hallmark of Burkitt's lymphoma[15] and is also found in 5% to 10% of DLBCLs.[16] The transgenic *Eμ-Myc* mouse model was generated to study the oncogenic role of MYC, and these mice develop clonal lymphomas and/or leukemias of pregerminal center (pre-GC) B-cell origin.[17,18] The mean latency is 110 days,[17,18] and the relatively long latency and clonality of the tumors implies that additional oncogenic lesions must occur in order to obtain complete transformation.

In humans, DLBCL is the most frequent form of non-Hodgkin lymphoma, accounting for 30% to 35% of all cases,[19] and is characterized as a clinically heterogeneous disease caused by a broad molecular diversity. Gene expression profiling has identified at least 3 major subtypes of DLBCL thought to reflect the cell of origin: GC B-cell–like (GCB), activated B-cell–like (ABC), and primary mediastinal B-cell lymphoma.[20,21] The ABC (in parallel to non-GCB) DLBCL subtype is associated with poorer overall survival compared with GCB and primary mediastinal B-cell lymphoma subtypes.[22] The demand for novel treatment modalities of DLBCL is high because up to one-third of DLBCL patients fail to respond to initial therapy or relapse soon after treatment.[22] Hence, more mechanistic insight is needed to decipher the molecular etiology of this disease and develop new therapeutic strategies.

We show here that *Prdm11* promotes lymphomagenesis in the *Eμ-Myc* mouse strain and that human DLBCLs with low levels of PRDM11 belong to the non-GCB subtype and correlate with shorter survival. Furthermore, identification of PRDM11 target genes indicates that transcriptional repression of *FOS* and *JUN* may be involved in the tumor suppressive mechanisms of PRDM11.

Methods

Plasmids and cloning

Genbank AK094792 complementary DNA (cDNA) FLJ37473 fis clone BRAWH2012540 was used as polymerase chain reaction (PCR) template to

Submitted March 5, 2014; accepted December 4, 2014. Prepublished online as *Blood* First Edition paper, December 12, 2014; DOI 10.1182/blood-2014-03-560805.

F.A., C.C., and K.T.J. contributed equally to this study.

The online version of this article contains a data supplement.

The publication costs of this article were defrayed in part by page charge payment. Therefore, and solely to indicate this fact, this article is hereby marked "advertisement" in accordance with 18 USC section 1734.

generate pcDNA-Flag-PRDM11. *PRDM11* cDNA was further subcloned into pGEX-4T-2 (Amersham), pRSET-A (Invitrogen), and pENTR3C (Invitrogen). *PRDM11* cDNA was transferred into gateway-modified forms of pCMV-HA, pBabe-puro-HA, and pAcGHLT-A (Pharmingen) plasmids by using standard cloning techniques or clonase protocols (Invitrogen). All final constructs were verified by sequence analysis. Plasmids used for transformation assays were pMSCV, pBabe-puro, pBabe-puro-GFP, and pLZRS-GFP-IRES-HA-MYC.[23]

Cell culture and transfections

The U2932 cell line was maintained in RPMI 1640 (Gibco), whereas HEK293, Phoenix-Eco, and HeLa cells were maintained in Dulbecco's modified Eagle medium (Gibco); all media contained 10% fetal calf serum (Biochrom), 100 U/mL penicillin, and 100 g/mL streptomycin (Invitrogen). Mouse embryonic fibroblasts (MEFs) were derived from E13.5 embryos and were used for assays within the second to fourth passages; wild-type (WT) and knockout (KO) MEFs were derived from the same litter.

Retrovirus production and MEF assays

Retroviral particles were obtained from transfected Phoenix-Eco cells and supplemented with polybrene (Sigma). For the short hairpin RNA (shRNA) library screen, MEFs were transduced with shRNAs, selected with puromycin, replated, and transduced with pLZRS-MYC-IRES-GFP/pLZRS-IRES-GFP. For colony formation assays, WT and KO MEFs were transduced with pBabe-MYC. MEFs were fixed with Lillie's fixative (Merck) and stained by crystal violet (Sigma).

For growth curves, transduced (pBabe-GFP/pBabe-HA-PRDM11) MEFs were puromycin-selected, seeded in quadruplicate, fixed with Lillie's fixative (Merck) at days 0 to 4, stained by crystal violet, dissolved by 10% acetic acid, and measured at 590 nm (GloMax Multi Detection System, Promega).

Generation and analysis of stable cell lines by lentiviral transduction

Lentiviral particles were harvested from HEK293 cells, transfected with pLKO-scramble (shScramble) or TRC2-358536 (shPRDM11) (Sigma-Aldrich), and used to transduce U2932 cells by spin infections on retronectin-coated plates. Cells were selected for 3 days by puromycin (Invitrogen).

Mice

Generation of the *Prdm11* KO mouse strain is described in supplemental Methods (available online at the *Blood* Web site). The Eμ-Myc transgenic mouse strain was obtained from The Jackson Laboratories and used to produce the *Eμ-Myc;Prdm11* KO mouse strain. Mice were examined twice a week for incidence of lymphoma and were euthanized when considered positive. All murine experiments were approved by Dyreforsoegstilsynet according to Danish legislation (license numbers 2008/561-1451 and 2013-15-2934-00811). Survival data were analyzed by using GraphPrism software.

Quantitative real-time PCR (qRT-PCR)

Total RNA was purified by using TRIzol (Invitrogen) or RNeasy (QIAGEN). Then, 1 to 2 μg of RNA was transcribed into cDNA (TaqMan Reverse Transcription Reagents, Applied Biosystems), and qRT-PCR was performed by using SYBR Green (Applied Biosystems) and analyzed by ABI Prism 7300 Sequence Detection System. The primer sequences are provided in supplemental Methods.

Magnetic-activated cell sorting and flow cytometry

For magnetic-activated cell sorting, cells obtained from freshly isolated spleen or bone marrow were sorted by using mouse CD45R/B220 microbeads according to the manufacturer's instructions (Miltenyi).

For cell cycle analysis, MEFs or freshly magnetic-activated cell sorted B cells ($B220^+$) were fixed overnight in ethanol, incubated with propidium iodide and RNaseA in 0.1% bovine serum albumin, and analyzed on a FACSCalibur flow cytometer (Becton-Dickinson). Data were analyzed by using FlowJo Software (TreeStar).

Eμ-Myc tumors underwent immunophenotyping. Cells from inguinal lymphomas or *Eμ-Myc*$^-$ controls were resuspended in fluorescence activated cell sorter (FACS) buffer (2% heat inactivated fetal bovine serum; 0.02% sodium azide in phosphate-buffered saline) containing Mouse BD Fc block (BD Biosciences), incubated with antibody-mix for 30 minutes, washed once, and resuspended in FACS buffer containing 4,6 diamidino-2-phenylindole (Invitrogen). Samples were kept on ice in the dark until they were analyzed by flow cytometry. Antibody combinations are described in the supplemental Methods. Flow cytometry was performed on an LSR-II cytometer (BD Biosciences), and data were analyzed with FlowJo software (TreeStar).

Immunoblotting and antibodies

Cells were lyzed in radioimmunoprecipitation assay buffer, and 5 to 20 μg of protein per lane was separated on 4% to 12% NuPAGE Bis-Tris gel (Invitrogen) and transferred to a nitrocellulose membrane (Amersham). A list of primary antibodies and the generation of α-PRDM11 antibodies is provided in supplemental Methods. Secondary antibodies were purchased at Vector Laboratories and detected by SuperSignal West Pico Chemiluminescent Substrate (Thermo Scientific).

Mouse tumor immunohistochemistry (IHC)

Sections were deparaffinized, heated for antigen retrieval, and incubated with primary antibodies (supplemental Methods). Secondary reagents were peroxidase-conjugated anti-rabbit immunoglobulin (Dako) or biotinylated polyclonal rabbit anti-rat immunoglobulin (Dako) in combination with streptavidin/horseradish peroxidase (Dako). Sections were lightly counterstained by hematoxylin. Microscopy was performed by using an Olympus BX51 microscope equipped with Color View soft imaging system for photomicrographs. Specimens of similarly prepared normal lymph nodes from C57BL/6 mice were used as controls.

Patient samples and IHC

Tumor specimens from newly diagnosed cases of DLBCL were obtained from patients diagnosed and treated at Rigshospitalet in Copenhagen, Denmark. Eighty-five formalin-fixed, paraffin-embedded and 100 fresh frozen lymphoma biopsies (see supplemental Table 2 for patients' characteristics) were available for analysis. The samples were selected according to availability of combined tumor tissue and clinical data. The majority were previously classified according to the Hans classification system into GCB or non-GCB subtypes based on IHC expression of BCL6, MUM1, and CD10.[24,25] Reactive lymph nodes were obtained from 5 individuals. Patient samples were taken before treatment, and all patients were treated with anthracycline-containing cyclophosphamide, doxorubicin, vincristine and prednisone (CHOP) or CHOP-like regimens; 9 patients also received rituximab. The clinical data were obtained from the patient files and from the Danish lymphoma registry (LYFO). Approval for this study was obtained from the ethics committee (H-KF-284246).

Polyclonal and monoclonal α-PRDM11 antibodies were evaluated in immunostainings of human reactive lymph nodes and thereafter used for immunostaining of DLBCL samples. Samples were counterstaining with hematoxylin. The intensity of PRDM11 staining, as well as the percentage of cells that exhibited positive staining for PRDM11, was used to calculate scores for PRDM11 IHC stains. Proportion of scores of positive cells: ≤10%, 1; >10% to ≤50%, 2; >50%, 3. Intensity scores ranged from 1 (weak), 2 (moderate), to 3 (strong). The scores for the percentage of positive cells and intensity were merged and grouped into 2 expression categories: $PRDM11^{low}$ (score ≤2) and $PRDM11^{high}$ (score >2), based on the observations that separation between intensity scores 2 and 3 was challenging. The stainings were scored independently by F.A. and E.R.

Statistical methods

Patient characteristics were reviewed in all of the DLBCL patients with reference to age, sex, stage at diagnosis, performance status, International Prognostic Index, and survival. Differences in clinical characteristics of patients with or without PRDM11 expression were evaluated by using the Pearson χ^2 or Fisher's exact tests. Overall survival was estimated by using the Kaplan-Meier method

from date of diagnosis to death or last follow-up. Last follow-up was 70 months. The equality between survival curves was tested with the log-rank test. Statistical analyses were performed in SPSS 18.0 for Windows (SPSS Inc.). Any differences were considered to be statistically significant when the P value was $<.05$.

FACS of B-cell subsets from tonsils

Cells were extracted from human tonsils, subjected to Lymphoprep separation of mononuclear cells, and stained for immunophenotyping by FACS (BD FACSAriaII) using an 8-color antibody combination (supplemental Methods). Analysis after sorting showed purity of >98%. RNA was extracted (RNAqueous-Micro, Ambion) from 4 distinct B-cell subsets: naïve B cells, GC CXCR4$^+$ centroblasts, GC CXCR4$^-$ centrocytes, and memory B cells.[26] A total of 20 ng RNA per sample was used for RT-PCR. qRT-PCR was performed as described above.

Chromatin immunoprecipitation (ChIP), ChIP–qRT-PCR, and ChIP-seq

U2932 cells were collected, cross-linked, and processed as previously described.[27] Samples were immunoprecipitated with polyclonal antibodies specific for PRDM11, RNA polymerase II (RNA pol II; sc-899X, Santa Cruz), or rabbit immunoglobulin G (IgG; Sigma). Eluted DNA was decross-linked and extracted by using the QIAquick PCR Purification Kit (QIAGEN) or MinElute PCR Purification Kit (QIAGEN). ChIP–qRT-PCR was performed by using SYBR Green (Applied Biosystems) and analyzed by using the ABI Prism 7300 Sequence Detection System. Primer sequences are provided in the supplemental Methods. For ChIP-seq analysis, DNA libraries were built by using NEBNext DNA Library Prep according to the manufacturer's instructions and analyzed by Solexa/Illumina high-throughput sequencing (100 cycles, single read). Description of data processing is provided in supplemental Methods. The data are deposited in the Gene Expression Omnibus database (accession number GSE56065).

RNA sequencing analysis

Total RNA was extracted from transduced U2932 cell lines selected with puromycin for 3 days using the RNeasy Plus kit and on-column DNAse digestion (QIAGEN). RNA was sequenced by using the HiSeq2000 system (Illumina). Data processing descriptions are provided in supplemental Methods. The data are deposited in the Gene Expression Omnibus database, accession number GSE56065.

Results

Functional screening identifies Prdm11 as a putative tumor suppressor

To identify novel SET/PR domain–encoding genes with tumor suppressive functions, we performed an oncogenic collaboration screen in MEFs by using a custom shRNA retroviral vector library in combination with MYC overexpression. The library contained 4 shRNA constructs toward each of 61 SET/PR-domain–encoding genes in the human and mouse genome. In total, 3 genes were identified as potential tumor suppressors in this screen: *Prdm11*, *Mll5*, and *Mecom/Prdm3*. We focus here on *Prdm11*. As seen in Figure 1A, shRNAs against *Prdm11* resulted in increased foci formation, particularly in cells with MYC overexpression.

PRDM11 locates to chromosome 11p11.2 in humans and encodes a gene with 6 coding exons that generate a protein with a PR domain, a nuclear localization signal, and a zinc knuckle motif (C-X_2-C-X_7-C-X_2-H-P-G) of unknown function[28] (Figure 1B). Unlike all other PRDMs,[3] PRDM11 does not contain zinc fingers. Both the gene structures and the amino acid sequences, except for the C-terminus, are highly conserved between humans and mice (Figure 1B and supplemental Figure 1A-B). In accordance with published data from human tissues,[3,29] murine *Prdm11* expression is generally low, with the highest expression in spleen, lung, mesenteric lymph node, and kidney (Figure 1C).

To investigate the tumor suppressive potential of *Prdm11* in vivo, we created a *Prdm11* KO mouse strain (supplemental Figure 1C-J). *Prdm11* KO mice are born in expected Mendelian ratios (supplemental Figure 1H), demonstrating that Prdm11 is not required for embryogenesis. Moreover, no apparent phenotype by gross pathological examinations was observed (data not shown), along with no difference in weight (supplemental Figure 1I) or survival (supplemental Figure 1J). Despite no genotype-specific differences in expression of key cell cycle regulators after MYC overexpression (supplemental Figure 2A), *Prdm11* KO MEFs showed increased oncogenic transformation capacity (Figure 1D), thus validating the findings of the shRNA library screen.

Overexpression of PRDM11 induces apoptosis

To characterize the function of PRDM11, we expressed exogenous human PRDM11 in MEFs. Overexpression of PRDM11 revealed an increase of cleaved caspase 3 (Figure 1E) and in line with an apoptotic phenotype, PRDM11-transduced MEFs had severely diminished cell growth (Figure 1F) and a large increase in the sub-G1 fraction (Figure 1G).

The tumor suppressor p53 induces apoptosis in response to sustained DNA damage and other cellular stresses, including deregulated MYC signaling.[30] Hence, we investigated whether PRDM11-induced apoptosis was p53-dependent by overexpressing PRDM11 in *p53* KO MEFs. Although *p53* KO MEFs proliferated faster than the *p53* WT cells, PRDM11 negatively affected the growth of both cell populations (Figure 1H) and induced cleavage of caspase 3 in the *p53* KO MEFs (Figure 1I), suggesting that loss of p53 is not sufficient to compensate for the effects of PRDM11 overexpression.

Because of the presence of a PR domain, we investigated whether PRDM11 possessed HMTase activity; however, such enzymatic activity could not be demonstrated (supplemental Figure 3A-B), suggesting that PRDM11 is not an intrinsic HMTase, that a required cofactor was not expressed in HEK293 cells, or that the target protein(s) of PRDM11 are nonhistones, as has recently been demonstrated for SMYD3.[31]

Loss of Prdm11 accelerates MYC-driven lymphomagenesis in vivo

As shown in Figure 1C, the highest expression of *Prdm11* messenger RNA was found in B-cell–rich compartments such as the spleen and lymph node. Sorting of splenocytes showed that PRDM11 was enriched in B220$^+$ cells confirming the expression of PRDM11 in B cells (Figure 2A). Western blotting using an α-PRDM11 monoclonal antibody revealed that besides the expected size of PRDM11 (≈55 kDa), 2 slower migrating forms of currently unknown nature are present in murine splenocytes, human lymphoma cells (Figure 2A), and HeLa cells (supplemental Figure 4A).

The relatively high level of PRDM11 in B cells implies that PRDM11 may play a functional role in this cell type. Because we have shown that *Prdm11* depletion enhances MYC-mediated transformation in vitro (Figure 1A,D), we used the *Eμ-Myc* mouse model to investigate a potential tumor suppressive function of *Prdm11* in vivo. As seen in Figure 2B, *Prdm11* deficiency significantly accelerated the development of *Eμ-Myc*–driven B-cell lymphomas, and the median survival was 113 and 94 days for *Eμ-Myc; Prdm11* WT and *Eμ-Myc;Prdm11* KO mice, respectively. We found

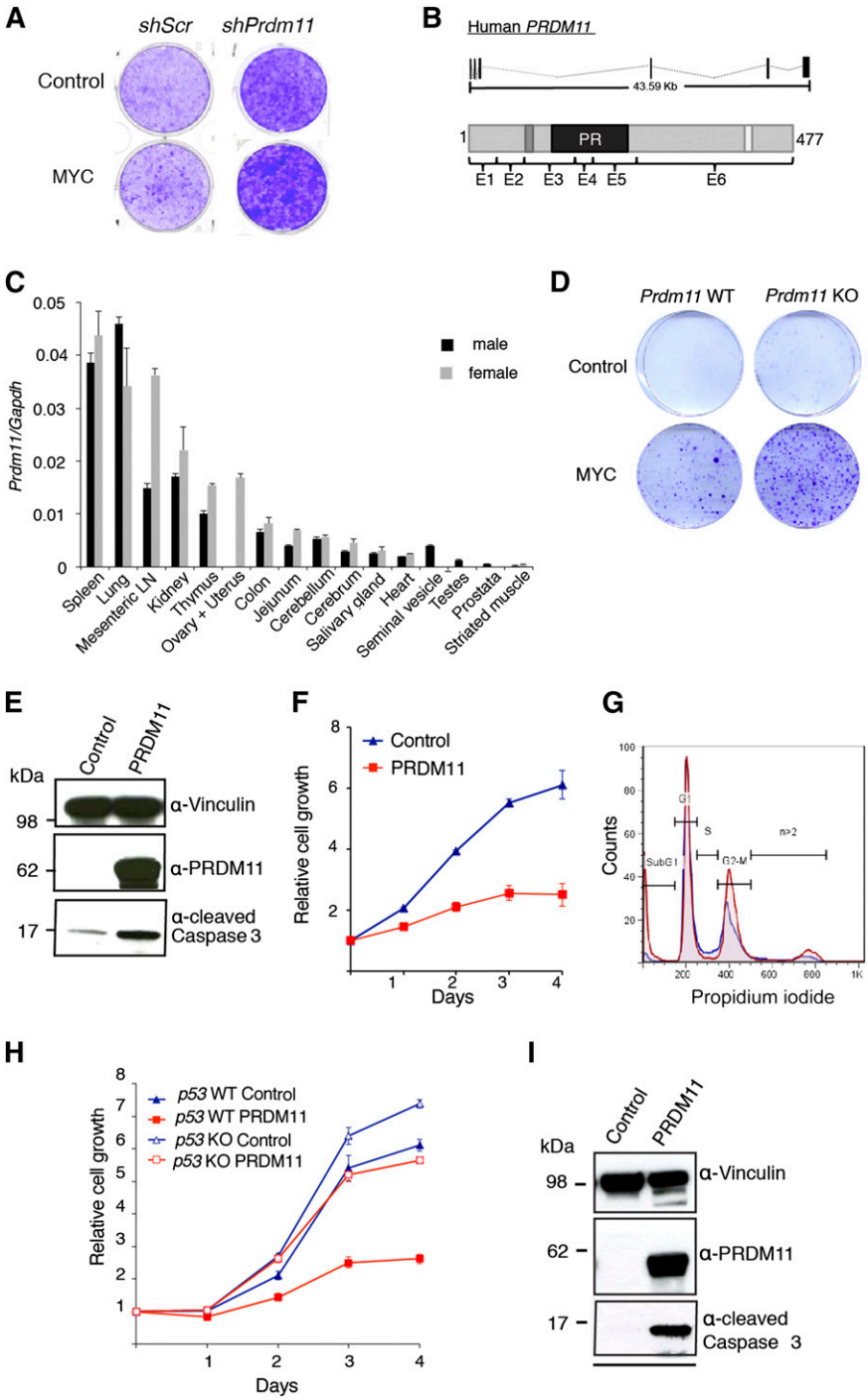

Figure 1. Characterization of the tumor suppressive potential of PRDM11. (A) Representative screening result showing focus formation assay of MEFs transduced with either scramble control shRNA or a pool of 4 shRNA constructs targeting *Prdm11* and subsequently transduced with either control (LZRS-GPF-IRES-HA) or MYC (LZRS-GPF-IRES-HA-MYC). (B) Schematic structure of *PRDM11* from human (NM_001256696) and the corresponding PRDM11 protein (NP_001243625.1). Protein coding exons are shown as vertical black lines and are indicated on the protein structures as E1 through E6. The positions of a zinc knuckle (dark gray), the PR domain (black), and a nuclear localization signal (white) are indicated. (C) Relative levels of *Prdm11* expression measured by qRT-PCR in a panel of tissues from male and female C57BL/6 mice. Levels of *Prdm11* were normalized to *Gapdh*. Error bars represent standard deviation (SD) of technical triplicates. (D) Colony formation assay of *Prdm11* WT or *Prdm11* KO MEFs transduced with either control (pBabe) or MYC (LZRS-GPF-IRES-HA-MYC). One representative experiment of 3 is shown. (E-F) MEFs were transduced with control (pBabe-GFP) or PRDM11 (pBabe-HA-PRDM11) and used for (E) immunoblotting (IB) of cleaved caspase 3. Middle panel confirms PRDM11 overexpression, and vinculin served as control for equal loading (n = 2). (F) Growth curves measured in quadruplicates by crystal violet staining; error bars denote SD; 1 representative experiment of 6 is shown. (G) Propidium iodide profiles of MEFs (n = 4) transduced with PRDM11 (red) or control vector (blue). (H-I) *p53* KO MEFs and *p53* WT MEFs were transduced with control (pBabe-GFP) or PRDM11 (pBabe-HA-PRDM11) and used for. (H) Growth curves measured in quadruplicates by using crystal violet staining. Error bars denote SDs; 1 representative experiment of 2 is shown. (I) IB analysis of *p53* KO MEFs. One representative experiment of 2 is shown. LN, lymph node.

no genotype-specific difference in tumor load on the day of euthanization (supplemental Figure 5A) or in proliferation measured by Ki67 immunostaining in a panel of *Eμ-Myc;Prdm11* WT and *Eμ-Myc;Prdm11* KO end-stage tumors derived from lymph nodes (Figure 2C and supplemental Figure 5B). B220 immunostaining was performed to confirm B-cell origin of the tumors. Although all (19 of 19) *Eμ-Myc*;*Prdm11* WT tumors were B220^{+}, 4 of 25 *Eμ-Myc*;*Prdm11* KO tumors were B220 $^{low/negative}$ (Figure 2C and supplemental Figure 5B). Because no tumors were CD3^{+} (Figure 2C and supplemental Figure 5B), this suggests that some *Eμ-Myc;Prdm11* KO tumors may de-differentiate or arise in a different stage of B-cell development compared with *Eμ-Myc;Prdm11* WT tumors. However, immuno-phenotyping by flow cytometry revealed no genotype-specific differences (Figure 2D and supplemental Figure 6A-B).

Spontaneous inactivation of the p53-p19^{ARF} pathway is frequently found in *Eμ-Myc* tumors[32]; however, *Prdm11* deficiency had no effect on the frequency of p53-p19^{ARF} inactivation (Figure 2E). We next investigated the level of PRDM11 in end-stage splenic tumors of WT background. PRDM11 was decreased in 5 of 14 *Eμ-Myc;Prdm11* WT tumors (Figure 2F, lanes 1, 3, 8, 12, and 13). The spontaneous downregulation of PRDM11 in *Eμ-Myc;Prdm11* WT lymphomas further supports a tumor suppressive role of PRDM11 in this mouse model.

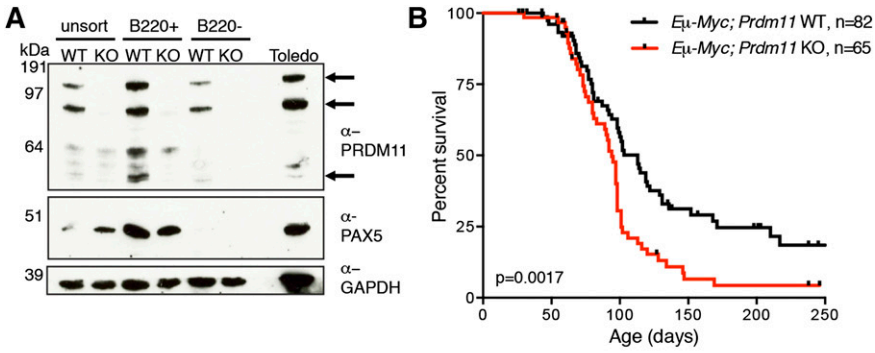

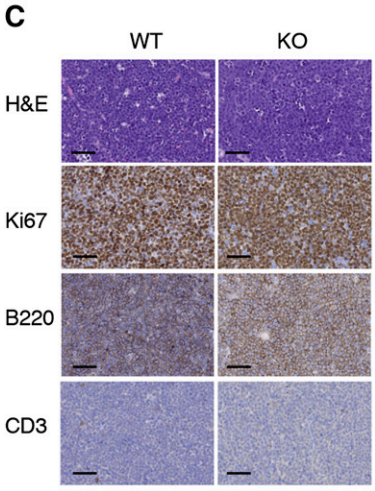

D

Genotype	ID	Tumor subtype
Prdm11-/- Eμ-Myc +/-	1910	T1
Prdm11-/- Eμ-Myc +/-	1986	T1 & plasma B cells
Prdm11-/- Eμ-Myc +/-	2072	immature B cells
Prdm11-/- Eμ-Myc +/-	2120	T1 & heterogeneous activated B cells
Prdm11-/- Eμ-Myc +/-	2029	T1 & plasma B cells
Prdm11-/- Eμ-Myc +/-	2041	pre-B
Prdm11-/- Eμ-Myc +/-	2047	pre-B
Prdm11-/- Eμ-Myc +/-	2055	pre-B
Prdm11-/- Eμ-Myc +/-	2113	T1 & heterogeneous CD19+ B220+ IgDint IgM+
Prdm11-/- Eμ-Myc +/-	2135	Plasma & heterogeneous activated B cells
Prdm11-/- Eμ-Myc +/-	2207	pre-B
Prdm11+/+ Eμ-Myc +/-	1968	T1
Prdm11+/+ Eμ-Myc +/-	1984	pre-B
Prdm11+/+ Eμ-Myc +/-	2038	pre-B
Prdm11+/+ Eμ-Myc +/-	2058	T1
Prdm11+/+ Eμ-Myc +/-	2060	T1
Prdm11+/+ Eμ-Myc +/-	2122	Plasma B cells
Prdm11+/+ Eμ-Myc +/-	2095	pre-B & heterogeneous activated B cells
Prdm11+/+ Eμ-Myc +/-	2097	pre-B & heterogeneous activated B cells
Prdm11+/+ Eμ-Myc +/-	2109	pre-B
Prdm11+/+ Eμ-Myc +/-	2211	Heterogeneous CD19+ B220+ IgDlow IgM+

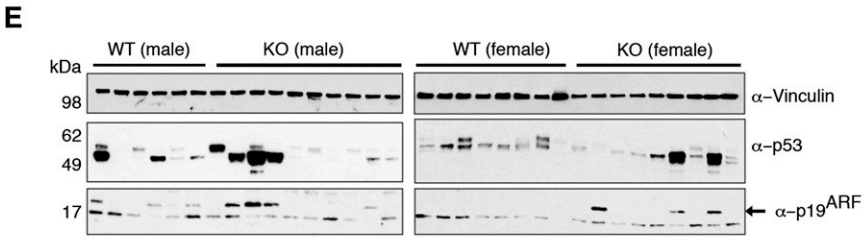

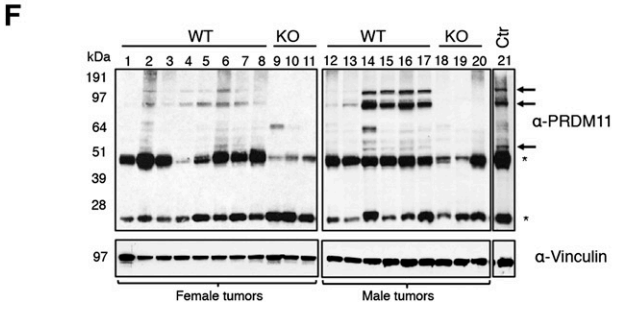

Figure 2. Loss of *Prdm11* accelerates MYC-induced lymphomagenesis in vivo. (A) IB of unsorted, B220$^+$, and B220$^-$ murine splenocytes from *Eμ-Myc$^-$;Prdm11* WT and *Eμ-Myc$^-$;Prdm11* KO mice. PAX5 was used as a sorting control and GAPDH served as a loading control. The arrows mark the 3 major PRDM11 protein species, which are also present in the human Toledo lymphoma cell line detected by α-PRDM11 monoclonal antibody (n = 2). (B) Kaplan-Meier plot of survival probability of *Eμ-Myc;Prdm11* WT (n = 82) and *Eμ-Myc;Prdm11* KO (n = 65) mice. Tumors occurred earlier in *Eμ-Myc$^+$;Prdm11* KO mice (P = .0017, log-rank test). (C) Representative micrographs of end-stage LN tumors from *Eμ-Myc;Prdm11* WT or *Eμ-Myc; Prdm11* KO mice immunostained with Ki67, B220, or CD3 antibodies. Scale bar = 50 μm. (D) Summary of immunophenotypes of lymphomas from mice with the indicated genotypes. T1: transitional T1 B cell. (E) IB analysis of the p53-p19^{ARF} pathway in a panel of end-stage splenic tumors from male (left) and female (right) *Eμ-Myc;Prdm11* WT or *Eμ-Myc;Prdm11* KO mice. High p53 protein levels, indicative of missense mutations in p53, were detected in 6 of 14 WT tumors and 8 of 20 KO tumors ($P > .05$, Fisher's exact test), whereas loss of p19^{ARF} was seen in 10 of 14 WT tumors and 13 of 20 KO tumors ($P > .05$, Fisher's exact test). Vinculin served as loading control. p19^{ARF} is marked by an arrow. The male and female tumors were run on separate gels. (F) IB of PRDM11 in a panel of splenic end-stage *EμMyc;Prdm11* WT tumors. *EμMyc;Prdm11* KO tumors and control (spleen from C57BL/6 mouse) were used as controls (Ctr) for the specificity of the α-PRDM11 monoclonal antibody. The 3 major PRDM11 protein species are indicated by arrows; asterisks mark endogenous immunoglobulin heavy and light chains. Vinculin served as loading control.

To identify deregulated oncogenic pathway(s) in B cells lacking PRDM11, we performed microarray analysis of *Eμ-Myc; Prdm11* WT and *Eμ-Myc;Prdm11* KO splenic end-stage tumors. Similar to results in previous reports,[33] end-stage tumors of the *Eμ-Myc* mouse display high heterogeneity (supplemental Figure 5C). Thus, only subtle differences in gene expression were identified ($\log_2$ FC 0.5; adjusted $P < .05$) (supplemental Table 1). The observation that tumors of the same genotype did not cluster together suggests that loss of *Prdm11* may increase the likelihood of transformation rather than perturbing a specific oncogenic pathway.

Because of increased *Myc* levels upon expression of the *Eμ-Myc* transgene in B cells, the premalignant B cells undergo a wave of proliferation accompanied by an increase in apoptosis. Many tumor suppressors therefore act to either increase the proliferation of the premalignant B cells, as observed following *p27* ablation,[34] or decreased apoptosis, such as *Bim*, *Bax*, or *Puma*.[35,36] To evaluate the effect of PRDM11 deficiency at the premalignant stage, B220$^+$ cells

from spleen or bone marrow of 30-day-old mice were examined, but no differences in cell cycle profiles or apoptotic index were observed (supplemental Figure 5D-G). In addition, the spleen weight ratio was unaffected by loss of *Prdm11* at the precancerous phase (supplemental Figure 5H).

PRDM11 expression in benign hyperplastic lymph nodes and DLBCLs

To investigate a role for PRDM11 in human tumors, 2 distinct antibodies (rabbit polyclonal and mouse monoclonal antibodies) were used for PRDM11 immunostaining of benign hyperplastic lymph nodes and DLBCLs. Similar staining patterns were observed for both antibodies (supplemental Figure 7A). In benign hyperplastic lymph nodes, PRDM11 exhibited high expression in GC cells in both the dark and light zones and was also expressed in scattered cells in the mantle zone and the interfollicular area (Figure 3A). Both nuclear and cytoplasmic staining of PRDM11 was observed (Figure 3A and supplemental Figure 7A). *PRDM11* expression was further evaluated in distinctive differentiation stages of B cell subtypes from benign tonsils; expression was seen in all sorted types of B cells, including naive B cells, centroblasts, centrocytes, and memory B cells (Figure 3B and supplemental Figure 7B-C).

To investigate a potential role of PRDM11 in human lymphomas, 85 primary human DLBCLs were analyzed for the expression of PRDM11 (Figure 3C and supplemental Table 2). DLBCLs were divided into 2 groups according to the level of PRDM11 expression (high or low) (see the "Methods" section). Importantly, low expression of PRDM11 significantly correlated with a lower overall survival time (Figure 3D).

Because tumor suppressor genes are often mutated or epigenetically downregulated in cancer, the DNA methylation status of the *PRDM11* promoter in primary patient samples was investigated. Promoter methylation was identified in 7 of 100 fresh-frozen primary lymphomas, whereas the locus in normal B cells was unmethylated (supplemental Figure 7D). Because our patient samples consisted of a combination of normal and malignant cells, we were not able to determine whether the promotor is fully methylated in tumor cells. However, there was no correlation between DNA methylation of the *PRDM11* promoter and expression level of PRDM11 as measured by immunostaining, which may be due to the relatively low number of methylated samples.

To investigate whether *PRDM11* is mutated in DLBCL, we analyzed 77 patient samples and matched normal tissue for point mutations in the coding sequence of *PRDM11*. Four different sequence variations were observed (supplemental Figure 7E), however since they occurred in nontumor tissue from the same patients, they are likely germline polymorphisms.

To investigate whether PRDM11 levels were associated with the GCB or non-GCB subtypes of DLBCL, the tumors were classified according to Hans algorithm[24] (supplemental Figure 7F) as previously described.[25] Interestingly, we found that although high PRDM11 expression was found with nearly equal frequency in GCB and non-GCB DLBCLs, 21 of 22 tumors with PRDM11 deficiency belonged to the non-GCB subtype (Figure 3E). Altogether, these data suggest that because *PRDM11* was expressed throughout B-cell development in the nonpathogenic lymph node and high PRDM11 levels were found in both GCB and non-GCB DLBCLs, the differential PRDM11 expression observed in DLBCL does not reflect an origin from a particular B-cell differentiation stage. Thus, PRDM11 may constitute an important novel risk predictor biomarker for aggressive behavior in DLBCL, in particular in the non-GCB subtype of DLBCL.

Identification of PRDM11 target genes

Because PRDMs are often involved in transcriptional regulation of target genes, we performed ChIP coupled with ChIP-seq in the U2932 DLBCL cell line by using 2 α-PRDM11 antibodies (Ab1 and Ab2) and an antibody for total RNA polymerase II. Ab1 and Ab2 bound 6,940 and 9,469 genomic regions, respectively. Of these, 2,229 were bound by both α-PRDM11 antibodies (supplemental Figure 8A and supplemental Table 3). The vast majority of these were located at the transcriptional start site (TSS) in gene bodies as well as in promoter regions (Figure 4A). Across all genes, PRDM11 binding was distributed throughout the length of target genes with the highest density around the TSSs, as was also found for RNA pol II (Figure 4B and supplemental Figure 8B). Moreover, most PRDM11 target genes were RNA pol II–positive (Figure 4C) and correlated with a high RNA pol II stalling index ($P = 5.1E-62$, Wilcoxon rank sum test) (Figure 4D), which is normally associated with genes responding to developmental or environmental cues.[37] Gene ontology analysis showed that PRDM11 target genes are involved in a variety of basic cellular processes, including metabolism and transcription (supplemental Figure 8C).

To validate the specificity of the α-PRDM11 antibodies used for ChIP-seq, 3 independent clones of U2932 cells depleted for *PRDM11* were generated (supplemental Figure 9A). Of note, depletion of PRDM11 for 28 days did not affect cell growth (supplemental Figure 9B-C). Both α-PRDM11 antibodies demonstrated specific enrichment of PRDM11 target genes, including *FOS* and *JUN* (Figure 4E and supplemental Figure 9D).

PRDM11 regulates the expression of cell cycle genes

To gain insight into how PRDM11 contributes to the regulation of target genes, we performed genome-wide expression analysis of PRDM11-depleted U2932 cells. We identified 649 significantly differentially expressed transcripts (supplemental Table 4); of these, 410 were downregulated and 239 were upregulated (supplemental Figure 9E), suggesting that PRDM11 can function as either a transcriptional repressor or an activator, depending on the specific promoter context. Interestingly, *FOS* was strongly upregulated upon knockdown of *PRDM11,* in line with the notion that the best scoring gene ontology categories were cell cycle and MAPKKK cascade (supplemental Figure 9F).

Overlapping the ChIP-seq and RNA-seq data sets identified 180 annotated genes that were bound by Ab1 and regulated by PRDM11 depletion (Figure 4F and supplemental Table 5). These represent ≈2.6% of the PRDM11 genomic binding sites identified by Ab1, and the low percentage may reflect that the ChIP-seq/RNA-seq experiments were performed in nonstimulated cells and PRDM11 "sits" on genes that are responsive to external stimuli. Interestingly, important oncogenes such as *FOS*, *JUN*, and *VAV3* were upregulated upon PRDM11 depletion, which we subsequently validated by qRT-PCR (Figure 4G). Together, these data suggest that PRDM11 binds chromatin around the TSS and regulates the expression of important target genes during lymphomagenesis.

Discussion

Here, we have identified *Prdm11* as a novel tumor suppressor by using a functional screening approach with MYC as the oncogenic driver. Because MYC is a major oncogene in human neoplasias,[14] identification of genes collaborating with MYC is key to understanding the

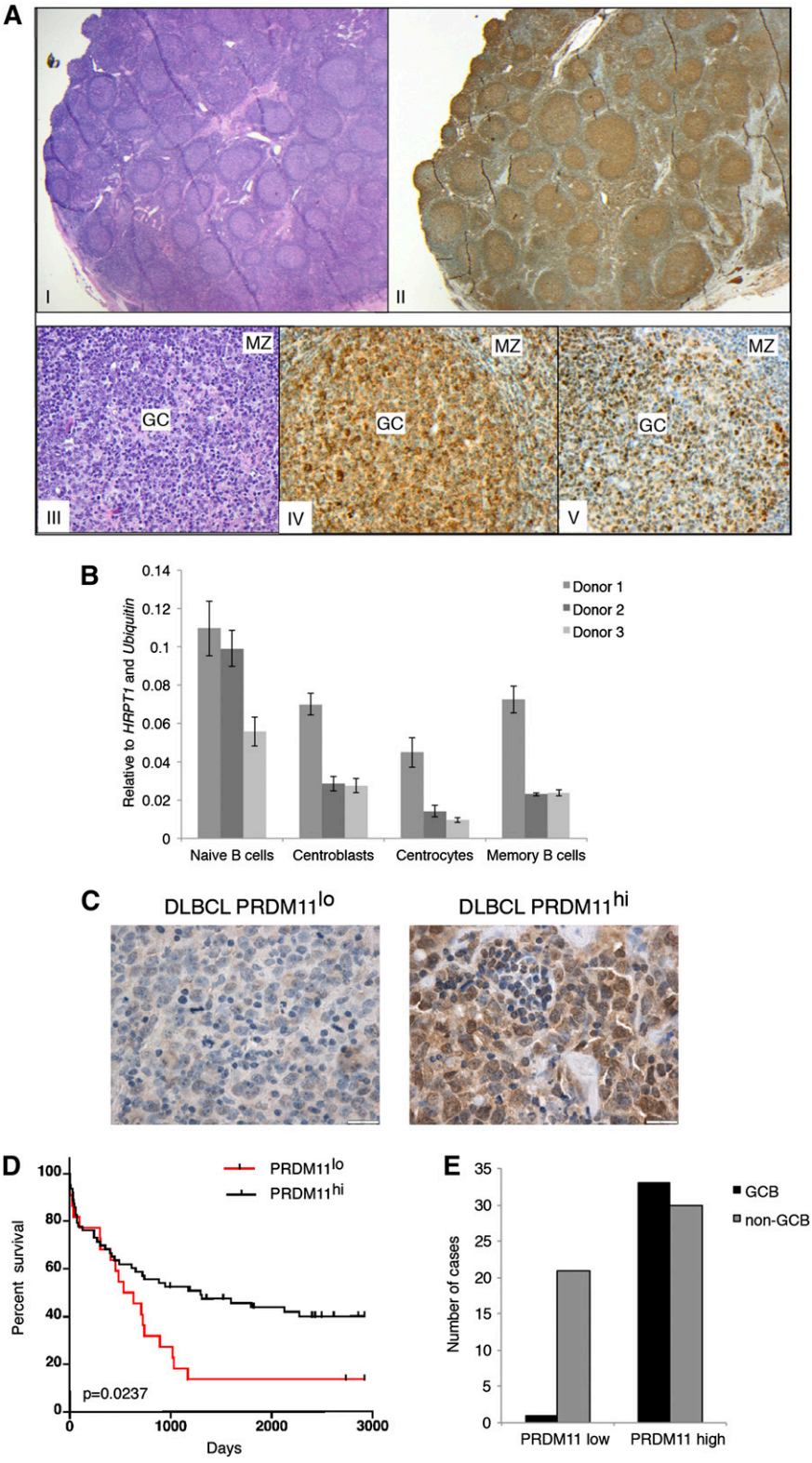

Figure 3. PRDM11 deficiency correlates with poorer survival in human DLBCL patients. (A) Human lymph node with follicular hyperplasia (I: hematoxylin and eosin (H&E); ×12.5) showing preferential labeling of PRDM11 in the germinal centers (II: PRDM11; ×12.5). The germinal center reaction is shown at a higher magnification (×200) in III; IV: H&E; V: PRDM11 staining of BCL6 illustrating that PRDM11 labels the GC (IV) similar to BCL6 (V), but also stains scattered small lymphocytes in the mantle zone (MZ). (B) Expression level of *PRDM11* in sorted B-cell populations from 3 human tonsils measured by qRT-PCR. (C) Representative α-PRDM11 immunostainings from human DLBCLs with either low PRDM11 (left; scale bar = 20 μm) or high PRDM11 (right; scale bar = 20 μm). (D) Kaplan-Meier survival curves comparing the survival of DLBCL patients according to PRDM11 levels. Patients with low levels of PRDM11 have significantly poorer survival ($P = .0237$, log-rank test). (E) Number of PRDM11^{lo} or PRDM11^{hi} DLBCLs according to GCB and non-GCB subtypes.

molecular etiology behind many cancers. Interestingly, the chromosomal region of *PRDM11* has previously been associated with tumor suppression,[38,39] and we demonstrate here, for the first time, a tumor suppressor role for *Prdm11* in vivo.

Although loss of *Prdm11* is not sufficient to mediate tumor development, this is consistent with the function of other PRDM family members. For instance B-cell–specific *Prdm1/Blimp1* KO mice develop B-cell–derived neoplasia only upon prolonged and repeated stimulation of the GC reaction.[40,41] We have identified that *Prdm11* is expressed in lymphoid tissues and, additionally, we have previously shown that despite a relatively high expression level of *Prdm11* in hematopoietic stem cells, *Prdm11*-ablated

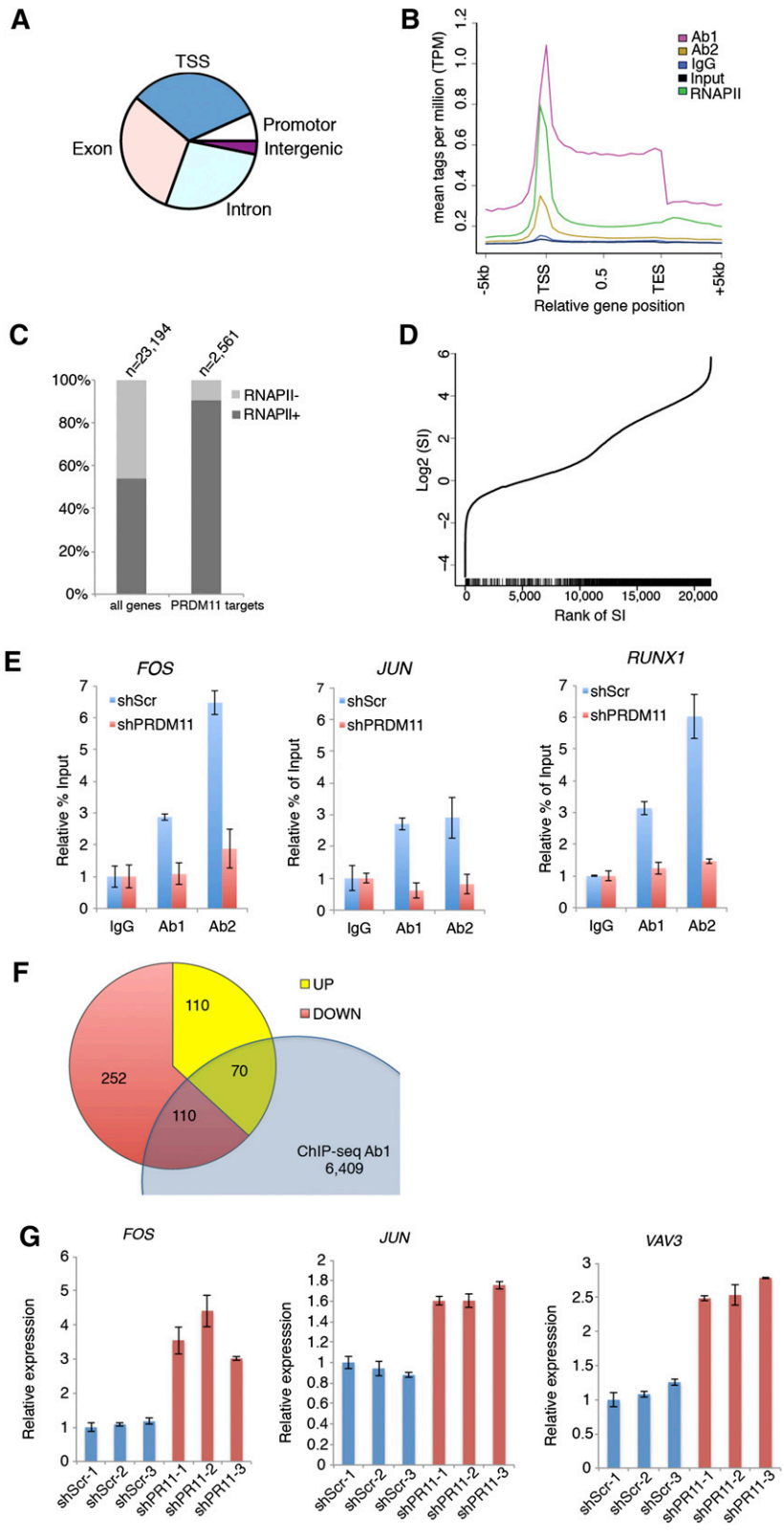

Figure 4. Identification of PRDM11 target genes. (A) Pie plot of the overall distribution of PRDM11 binding sites in U2932 cells into TSS, promoter, exon, intron, and intergenic regions. (B) Mean distribution of tags across gene bodies for both PRDM11 antibodies, IgG, input, and total RNA polymerase II (RNAPII). (C) Histogram showing the distribution according to RNA polymerase II status of all genes and PRDM11 target genes ($P < .01$, Fisher's exact test). (D) Graph illustrating the rank of genes according to RNA polymerase II stalling index (SI) (x-axis) plotted against the $\log_2$ SI (y-axis). Vertical black bars on the x-axis mark the positions of PRDM11 targets, which correlate with stalled genes ($P = 5.1E-62$, Wilcoxon rank sum test). (E) Examples of ChIP-qRT-PCR results in control (shScr) or PRDM11-depleted (shPRDM11) U2932 cells. Percent of enrichment was calculated and normalized to the IgG control of each cell line. Mean ± SD of technical triplicates is shown. (F) Venn diagram showing the overlap between PRDM11 target genes bound by Ab1 and annotated genes upregulated or downregulated by *PRDM11* shRNA in U2932 cells ($\log_2$FC0.5, false discovery rate ≤0.05). (G) qRT-PCR validation of selected genes from the overlap between ChIP-seq and RNA-seq analysis of PRDM11-depleted U2932 cells (red) vs control cells (blue). Each messenger RNA was normalized to the average of the housekeeping genes *β-actin*, *Ubiquitin*, *36B4*, and *GAPDH* and is shown relative to shScramble-1. Mean ± SD of technical triplicates is shown. *FOS*, $P = .015$; *JUN*, $P = .003$; and *VAV3*, $P = .0005$ (unpaired, two-tailed Student *t* test).

hematopoietic stem cells are fully functional in regenerating the hematopoietic system.[42] This study also revealed a negative effect on B-cell and T-cell generation upon loss of *Prdm11*, indicating that *Prdm11* could play a role in lymphoid differentiation. However, because *Prdm11* is also expressed in other cell types, we cannot exclude the possibility that tumor suppression could involve other mechanisms, such as immune surveillance defects in the *Eμ-Myc;Prdm11* KO mouse.

Our data from *Eμ-Myc* mouse tumors and *p53* KO MEFs suggests that PRDM11 does not mediate its tumor-suppressive effect via the p53 pathway. Interestingly, PRDM11 may still be involved in cell cycle control because many of the identified PRDM11 target genes are cell

cycle regulators. However, loss of *Prdm11* did not affect proliferation of the bulk population of $B220^+$ cells from either *Prdm11* KO mice or from premalignant *Eμ-Myc;Prdm11* KO mice, suggesting that *Prdm11* may be important for cell cycle progression of a specific stage of B-cell differentiation or following specific stimuli. In addition, depletion of *PRDM11* in human lymphoma cell lines did not affect cell proliferation.

PRDM11 contains a PR domain, which has been associated with HMTase activity in other PRDM family members;[6-9] however, we were unable to detect such enzymatic activity for PRDM11. This is in accordance with other PRDMs, such as PRDM1[43,44] and PRDM5,[27,45] which regulate target genes by recruitment of cofactors involved in transcription or epigenetic gene regulation. Here, we provide the evidence that PRDM11 is involved in transcriptional regulation of target genes in human DLBCL cells. In contrast to other PRDMs with a defined DNA binding consensus sequence, such as PRDM5,[27,45] PRDM9,[46,47] and PRDM14,[48,49] a putative DNA binding consensus sequence for PRDM11 could not be identified, suggesting that PRDM11 does not bind directly to target loci but is brought to the TSS by 1 or more as yet unidentified binding partners. Since the AP-1 transcription factor genes *FOS* and *JUN* are among the genes repressed by PRDM11, we speculate that the tumor suppressive mechanism of PRDM11 could involve transcriptional repression of genes that are normally induced by aberrant growth factor signaling or oncogenic activation of MAP kinase signaling, such as constitutively active RAS.[50]

PRDM1/BLIMP1 is known to be the master regulator of the final differentiation steps of plasma cells[51] and a tumor suppressor of the ABC-like subtype of DLBCL.[10,11] Here we show that low expression of another PRDM family member, PRDM11, also correlates with poor survival of DLBCL patients and that PRDM11 deficiency was identified almost exclusively in patients belonging to the non-GCB subtype. This suggests that low levels of PRDM11 could constitute a novel biomarker for risk prediction in DLBCL and a potential marker for distinction between GCB and non-GCB DLBCLs. Today, DLBCL is treated with CHOP chemotherapy in combination with the monoclonal α-CD20 receptor antibody rituximab (R-CHOP).[22] An interesting future task will be to address whether PRDM11 levels could be predictive of treatment responses.

In summary, we show for the first time that *Prdm11* is a tumor suppressor of MYC-induced lymphoma and that PRDM11 is a transcriptional regulator. We furthermore demonstrate a clinical relevance for PRDM11 in DLBCL, which implies that PRDM11 could be used as a marker of non-GCB DLBCL and paves the way for future understanding of B-cell pathology.

Acknowledgments

The authors thank Jesper Christensen and Heidi Huddlebusch for providing recombinant GST-PRDM11 and GST-MMSET, respectively, Shuchi Agrawal-Singh and Nikolaj Dietrich for providing ChIP-qRT-PCR primers, and Kim Jensen and Janine Erler for helpful inputs during manuscript preparation.

This work was supported by the Novo Nordisk Foundation, the Danish National Research Foundation, the Association for International Cancer Research, the Danish Medical Research Council, and the Danish Cancer Society. C.K.F. was supported by a personal grant from the Danish Cancer Society.

Authorship

Contribution: C.K.F., F.A., C.C., K.T.J., A.L., A.K.B., M.v.L., K.G., and A.H.L. conceived and designed the experiments; C.K.F., F.A., C.C., K.T.J., T.B.K., L.J., A.L., L.R., N.F.Ø., H.V.M., K.A., A.K.B., E.R., K.G., and A.H.L. performed the experiments; C.F.K., F.A., C.C., K.T.J., J.V.J., A.L., C.F., A.K.B., E.R., K.G., and A.H.L. analyzed the data; and C.K.F., F.A., C.C., J.V.J., K.G., and A.H.L. wrote the paper.

Conflict-of-interest disclosure: The authors declare no competing financial interests.

Correspondence: Anders H. Lund, Biotech Research and Innovation Center, University of Copenhagen, Ole Maaloes Vej 5, DK-2200 Copenhagen N, Denmark; e-mail: anders.lund@bric.ku.dk.

References

1. Fog CK, Galli GG, Lund AH. PRDM proteins: important players in differentiation and disease. *BioEssays.* 2012;34(1):50-60.
2. Hohenauer T, Moore AW. The Prdm family: expanding roles in stem cells and development. *Development.* 2012;139(13):2267-2282.
3. Fumasoni I, Meani N, Rambaldi D, Scafetta G, Alcalay M, Ciccarelli FD. Family expansion and gene rearrangements contributed to the functional specialization of PRDM genes in vertebrates. *BMC Evol Biol.* 2007;7:187.
4. Sun X-J, Xu P-F, Zhou T, et al. Genome-wide survey and developmental expression mapping of zebrafish SET domain-containing genes. *PLoS ONE.* 2008;3(1):e1499.
5. Huang S, Shao G, Liu L. The PR domain of the Rb-binding zinc finger protein RIZ1 is a protein binding interface and is related to the SET domain functioning in chromatin-mediated gene expression. *J Biol Chem.* 1998;273(26):15933-15939.
6. Kim K-C, Geng L, Huang S. Inactivation of a histone methyltransferase by mutations in human cancers. *Cancer Res.* 2003;63(22):7619-7623.
7. Pinheiro I, Margueron R, Shukeir N, et al. Prdm3 and Prdm16 are H3K9me1 methyltransferases required for mammalian heterochromatin integrity. *Cell.* 2012;150(5):948-960.
8. Eom G-H, Kim K, Kim S-M, et al. Histone methyltransferase PRDM8 regulates mouse testis steroidogenesis. *Biochem Biophys Res Commun.* 2009;388(1):131-136.
9. Hayashi K, Yoshida K, Matsui Y. A histone H3 methyltransferase controls epigenetic events required for meiotic prophase. *Nature.* 2005;438(7066):374-378.
10. Tam W, Gomez M, Chadburn A, Lee JW, Chan WC, Knowles DM. Mutational analysis of PRDM1 indicates a tumor-suppressor role in diffuse large B-cell lymphomas. *Blood.* 2006;107(10):4090-4100.
11. Pasqualucci L, Compagno M, Houldsworth J, et al. Inactivation of the PRDM1/BLIMP1 gene in diffuse large B cell lymphoma. *J Exp Med.* 2006;203(2):311-317.
12. Galli GG, Multhaupt HA, Carrara M, et al. Prdm5 suppresses Apc(Min)-driven intestinal adenomas and regulates monoacylglycerol lipase expression. *Oncogene.* 2014;33(25):3342-3350.
13. Watanabe Y, Toyota M, Kondo Y, et al. PRDM5 identified as a target of epigenetic silencing in colorectal and gastric cancer. *Clin Cancer Res.* 2007;13(16):4786-4794.
14. Meyer N, Penn LZ. Reflecting on 25 years with MYC. *Nat Rev Cancer.* 2008;8(12):976-990.
15. Hummel M, Bentink S, Berger H, et al; Molecular Mechanisms in Malignant Lymphomas Network Project of the Deutsche Krebshilfe. A biologic definition of Burkitt's lymphoma from transcriptional and genomic profiling. *N Engl J Med.* 2006;354(23):2419-2430.
16. Savage KJ, Johnson NA, Ben-Neriah S, et al. MYC gene rearrangements are associated with a poor prognosis in diffuse large B-cell lymphoma patients treated with R-CHOP chemotherapy. *Blood.* 2009;114(17):3533-3537.
17. Adams JM, Harris AW, Pinkert CA, et al. The c-myc oncogene driven by immunoglobulin enhancers induces lymphoid malignancy in transgenic mice. *Nature.* 1985;318(6046):533-538.
18. Harris AW, Pinkert CA, Crawford M, Langdon WY, Brinster RL, Adams JM. The E mu-myc transgenic mouse. A model for high-incidence spontaneous

lymphoma and leukemia of early B cells. *J Exp Med.* 1988;167(2):353-371.

19. Siegel R, Naishadham D, Jemal A. Cancer statistics, 2013. *CA Cancer J Clin.* 2013;63(1): 11-30.
20. Alizadeh AA, Eisen MB, Davis RE, et al. Distinct types of diffuse large B-cell lymphoma identified by gene expression profiling. *Nature.* 2000; 403(6769):503-511.
21. Rosenwald A, Wright G, Leroy K, et al. Molecular diagnosis of primary mediastinal B cell lymphoma identifies a clinically favorable subgroup of diffuse large B cell lymphoma related to Hodgkin lymphoma. *J Exp Med.* 2003;198(6):851-862.
22. Roschewski M, Staudt LM, Wilson WH. Diffuse large B-cell lymphoma-treatment approaches in the molecular era.; *Nat Rev Clin Oncol.* 2014;11 (1):12-23.
23. Jacobs JJ, Scheijen B, Voncken JW, Kieboom K, Berns A, van Lohuizen M. Bmi-1 collaborates with c-Myc in tumorigenesis by inhibiting c-Myc-induced apoptosis via INK4a/ARF. *Genes Dev.* 1999;13(20):2678-2690.
24. Hans CP, Weisenburger DD, Greiner TC, et al. Confirmation of the molecular classification of diffuse large B-cell lymphoma by immunohistochemistry using a tissue microarray. *Blood.* 2004;103(1):275-282.
25. Sjö LD, Poulsen CB, Hansen M, Møller MB, Ralfkiaer E. Profiling of diffuse large B-cell lymphoma by immunohistochemistry: identification of prognostic subgroups. *Eur J Haematol.* 2007;79(6):501-507.
26. Caron G, Le Gallou S, Lamy T, Tarte K, Fest T. CXCR4 expression functionally discriminates centroblasts versus centrocytes within human germinal center B cells. *J Immunol.* 2009;182(12): 7595-7602.
27. Galli GG, Honnens de Lichtenberg K, Carrara M, et al. Prdm5 regulates collagen gene transcription by association with RNA polymerase II in developing bone. *PLoS Genet.* 2012;8(5): e1002711.
28. Briknarová K, Atwater DZ, Glicken JM, Maynard SJ, Ness TE. The PR/SET domain in PRDM4 is preceded by a zinc knuckle. *Proteins.* 2011;79(7): 2341-2345.
29. Loth DW, Artigas MS, Gharib SA, et al. Genome-wide association analysis identifies six new loci associated with forced vital capacity. *Nat Genet.* 2014;46(7):669-677.
30. Vousden KH, Prives C. Blinded by the Light: The Growing Complexity of p53. *Cell.* 2009;137(3): 413-431.
31. Mazur PK, Reynoird N, Khatri P, et al. SMYD3 links lysine methylation of MAP3K2 to Ras-driven cancer. *Nature.* 2014;510(7504):283-287.
32. Eischen CM, Weber JD, Roussel MF, Sherr CJ, Cleveland JL. Disruption of the ARF-Mdm2-p53 tumor suppressor pathway in Myc-induced lymphomagenesis. *Genes Dev.* 1999;13(20): 2658-2669.
33. Mori S, Rempel RE, Chang JT, et al. Utilization of pathway signatures to reveal distinct types of B lymphoma in the Emicro-myc model and human diffuse large B-cell lymphoma. *Cancer Res.* 2008; 68(20):8525-8534.
34. Martins CP, Berns A. Loss of p27(Kip1) but not p21(Cip1) decreases survival and synergizes with MYC in murine lymphomagenesis. *EMBO J.* 2002;21(14):3739-3748.
35. Egle A, Harris AW, Bouillet P, Cory S. Bim is a suppressor of Myc-induced mouse B cell leukemia. *Proc Natl Acad Sci USA.* 2004;101(16): 6164-6169.
36. Eischen CM, Roussel MF, Korsmeyer SJ, Cleveland JL. Bax loss impairs Myc-induced apoptosis and circumvents the selection of p53 mutations during Myc-mediated lymphomagenesis. *Mol Cell Biol.* 2001;21(22): 7653-7662.
37. Price DH. Poised polymerases: on your mark...get set...go! *Mol Cell.* 2008;30(1):7-10.
38. Ricketts SL, Carter JC, Coleman WB. Identification of three 11p11.2 candidate liver tumor suppressors through analysis of known human genes. *Mol Carcinog.* 2003;36(2):90-99.
39. Ruivenkamp CAL, van Wezel T, Zanon C, et al. Ptprj is a candidate for the mouse colon-cancer susceptibility locus Scc1 and is frequently deleted in human cancers. *Nat Genet.* 2002;31(3): 295-300.
40. Calado DP, Zhang B, Srinivasan L, et al. Constitutive canonical NF-κB activation cooperates with disruption of BLIMP1 in the pathogenesis of activated B cell-like diffuse large cell lymphoma. *Cancer Cell.* 2010;18(6):580-589.
41. Mandelbaum J, Bhagat G, Tang H, et al. BLIMP1 is a tumor suppressor gene frequently disrupted in activated B cell-like diffuse large B cell lymphoma. *Cancer Cell.* 2010;18(6):568-579.
42. Thoren LA, Fog CK, Jensen KT, et al. PRDM11 is dispensable for the maintenance and function of hematopoietic stem and progenitor cells. *Stem Cell Res (Amst).* 2013;11(3):1129-1136.
43. Gyory I, Wu J, Fejér G, Seto E, Wright KL. PRDI-BF1 recruits the histone H3 methyltransferase G9a in transcriptional silencing. *Nat Immunol.* 2004;5(3):299-308.
44. Yu J, Angelin-Duclos C, Greenwood J, Liao J, Calame K. Transcriptional repression by blimp-1 (PRDI-BF1) involves recruitment of histone deacetylase. *Mol Cell Biol.* 2000;20(7): 2592-2603.
45. Duan Z, Person RE, Lee H-H, et al. Epigenetic regulation of protein-coding and microRNA genes by the Gfi1-interacting tumor suppressor PRDM5. *Mol Cell Biol.* 2007;27(19):6889-6902.
46. Baudat F, Buard J, Grey C, et al. PRDM9 is a major determinant of meiotic recombination hotspots in humans and mice. *Science.* 2010; 327(5967):836-840.
47. Myers S, Bowden R, Tumian A, et al. Drive against hotspot motifs in primates implicates the PRDM9 gene in meiotic recombination. *Science.* 2010;327(5967):876-879.
48. Ma Z, Swigut T, Valouev A, Rada-Iglesias A, Wysocka J. Sequence-specific regulator Prdm14 safeguards mouse ESCs from entering extraembryonic endoderm fates. *Nat Struct Mol Biol.* 2011;18(2):120-127.
49. Chia N-Y, Chan Y-S, Feng B, et al. A genome-wide RNAi screen reveals determinants of human embryonic stem cell identity. *Nature.* 2010; 468(7321):316-320.
50. Pylayeva-Gupta Y, Grabocka E, Bar-Sagi D. RAS oncogenes: weaving a tumorigenic web. *Nat Rev Cancer.* 2011;11(11):761-774.
51. Turner CA Jr, Mack DH, Davis MM. Blimp-1, a novel zinc finger-containing protein that can drive the maturation of B lymphocytes into immunoglobulin-secreting cells. *Cell.* 1994;77(2): 297-306.